Effect of substrate strain on calculated magnetic properties and magnetic anisotropy energy of CoO

A. Boussendel,[1,2] N. Baadji,[3] A. Haroun,[4] H. Dreyssé,[1] and M. Alouani[1]

[1]*Institut de Physique et de Chimie des Matériaux de Strasbourg (IPCMS), UMR 7504, UdS–CNRS, 23 rue du Loess, 67034 Strasbourg, France, EU*

[2]*Département de Physique, Faculté des Sciences, Université de M'sila, 28000 M'sila, Algeria*

[3]*School of Physics and CRANN, Trinity College, Dublin 2, Ireland*

[4]*LPQSD, Département de Physique, Université Ferhat Abbas, Sétif, Algeria*

(Received 17 November 2009; revised manuscript received 13 April 2010; published 25 May 2010)

The electronic structure, magnetic properties, and magnetic anisotropy energy (MAE) of the insulating antiferromagnetic bulk CoO and CoO strained by silver or MnO substrates have been studied by means of three different methods: (1) a simple model based on the crystal-field approach, (2) the full-potential linear augmented plane-waves method within the generalized gradient approximation (GGA), and (3) the so-called GGA+U method. In all methods the spin-orbit coupling is included. In the third method, the Hubbard interaction U is used to treat the strong electron-electron interaction due to the cobalt localized open d shell. The results of the various calculations for bulk CoO and those of CoO strained by silver or MnO substrates are discussed and compared with available experimental data and other calculations. The GGA predicts incorrectly that bulk CoO is a metallic oxide and its spin magnetic moment is oriented along the inclination angle θ of 66° and the azimuth angle ϕ of 45° and the hard axis along the c direction. The orbital magnetic moment is also much smaller compared to experiment. On the contrary, within the GGA+U bulk CoO becomes an insulator as expected and the spin magnetic moment is oriented along the tetragonal c axis; it rotates in plane when CoO is strained by a silver substrate, and out of plane when strained by an MnO substrate. Within the GGA+U an unquenched orbital magnetic moment on the order of $1\mu_B$ is obtained in both bulk CoO and CoO strained by MnO substrate but is much smaller ($0.45\mu_B$) when CoO is strained by silver. All these results together with the values of MAE are in good agreement with experiment and our crystal-field analysis.

DOI: 10.1103/PhysRevB.81.184432 PACS number(s): 75.70.−i, 71.15.Nc, 71.70.Fk, 71.20.−b

I. INTRODUCTION

The early transition-metal (TM) monoxides occupy a special place in condensed-matter physics, first, because of their potential technological applications and, second, because they are commonly considered as the prototype of the Mott-insulator concept. Since the insulating properties of these TM monoxides, both below and above the Néel temperature, were not explained by a band model,[1] the importance of the electron-electron interaction has been discussed. It is generally agreed that the large Coulomb interaction causes the insulating ground state.[2,3] The insulating character of the TM monoxides seems to be initially in contradiction with their electronic configuration where the metal s states are empty and the oxygen p orbitals are filled and far from the Fermi level while the d shell is partially filled. From the partial occupations of the d shell, one expects naively that these compounds are conductors. However, the strong partially unscreened electron-electron interaction reconciles their electronic structure with their insulating behavior and explains why the density-functional theory (DFT) within the local-spin-density approximation (LSDA) failed to describe such a complex electronic structure. For example, the LSDA predicted CoO and FeO to be metals and MnO and NiO to be semiconductors with small band gaps.[4] This failure is due mainly to the lack of proper accounting for the strong electronic correlation.

The problem with the LSDA is the inability to split the occupied states of the TM monoxides from their empty states so that the energy separation reaches the experimental band gap. Several attempts have been made to improve the LSDA, such as the generalized gradient approximation[5] (GGA), the self-interaction correction[6–8] (SIC), the orbital polarized correction,[9] and the local-spin-density approximation corrected by the Coulomb interaction U, the so-called LSDA +U method.[10–18] The GGA introduced by Perdew *et al.*[5] adds to some extend the nonlocality of the electron-electron correlation by making a functional not only of the density but also of its gradient. It was applied without much success by Engel *et al.*[19] and Dufek *et al.*[20] to CoO to reproduce its insulating antiferromagnetic (AFM) ground state. Svane and Gunnarsson[6] applied a fully self-consistent, *ab initio* LSDA +SIC to the AFM CoO to eliminate the spurious interaction of an electron with itself from the conventional DFT-LSDA formulation. The band gap and the magnetic moment were improved when compared with the LSDA results. Using the LSDA+U, Wei and Qi[21] found that these oxides are insulating. More interesting recent study by Eschrig *et al.*[22] of high spin-low spin transition under pressure of CoO by this latter method showed that the collapse of magnetic moment was due to a competition between the ligand field and intra-atomic exchange. However the method failed to predict the insulator-to-metal transition under pressure.

CoO is an antiferromagnetic TM monoxide insulator with a Néel temperature T_N of about 291 K.[23] It has been shown that above T_N CoO orders in a simple rocksalt crystal structure[23] (space group $Fm3m$) and there is no evidence for a previously reported small tetragonal elongation.[24] Below

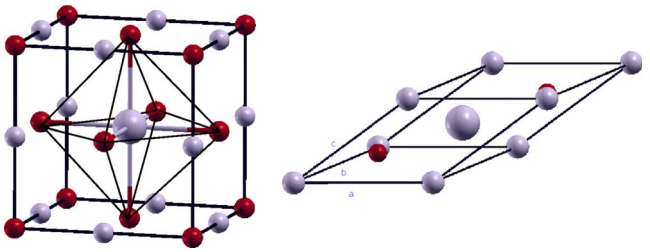

FIG. 1. (Color online) NaCl structure of CoO in its paramagnetic (left) state and magnetic cell of AFM-II of CoO (right). The atoms of oxygen are in red (dark gray) and cobalt in gray. The central Co atom is shown as a bigger ball to highlight the cobalt and oxygen octahedron.

T_N, CoO is subjected to a tetragonal contraction of 1.2% at 0 K.[23,25] The magnetic configuration below T_N is an antiferromagnetic type-II where the atomic magnetic moments are arranged in ferromagnetic sheets parallel to (111) planes with alternate signs in successive sheets. This AFM-II magnetic structure can be described with a doubled rhombohedral unit cell (if we neglect the tetragonal distortion as shown in Fig. 1) which leads to the space group $R\bar{3}m(D_{3d})$.

In the rocksalt structure, the d orbital splits into a triplet $t_{2g}(\Gamma_5)$ and a doublet $e_g(\Gamma_3)$. The orbital associated to the triplet are d_{xy}, d_{xz}, and d_{yz} and those of the doublet are $d_{x^2-y^2}$ and $d_{3z^2-r^2}$. This reduction in symmetry to a rhombohedral symmetry $R\bar{3}m(D_{3d})$ leads to splitting of the triplet t_{2g} into a doublet e_g' and a singlet a_g and in addition the two doublets e_g and e_g' are mixed. The a_g orbital is the rhombohedral $d_{3z'^2-r^2}$ orbital, equivalent to the cubic t_{2g} linear combination $(d_{xy}+d_{xz}+d_{yz})/\sqrt{3}$. The orbitals associated to the doublet e_g' are a linear combination of mainly of the cubic d_{xy}, d_{xz}, and d_{yz}, with a small contribution (10%) form the cubic e_g orbital, while the doublet e_g mixes slightly with the t_{2g} orbitals. Experiments[26] suggest that in addition of the tetragonal distortion there is an extra rhombohedral distortion along the (111) axis of the cubic phase. Both distortions combined lead to a further reduction in the symmetry of CoO to a triclinic. In this triclinic phase, the doublets E and E' split further to two singlets and all the degeneracy of d orbital is lifted.

From a theoretical point of view CoO is an interesting material because it is one of the few materials that have a large magnetic orbital moment m_l. This results in a strong coupling between the spin and orbital magnetic moments through the spin-orbit coupling[27–30] (SOC). In most of transition metal systems, the orbital magnetic moment is quenched and is therefore much smaller compared to the spin magnetic moment. The presence of the large m_l in AFM CoO was invoked to interpret the magnetic susceptibility[31] and the neutron scattering.[32] A large m_l of about $1\mu_B$ is also obtained by Jo and Shishidou[33] in the isotropic $L_{2,3}$ x-ray absorption spectroscopy spectrum for Co^{2+} and Fe^{2+} ions in the octahedral (O_h) crystal field. In his study of antiferromagnetic arrangement of magnetic moments in CoO by neutron diffraction, Roth[25] found that the spin direction is oriented in the $[\bar{1}\bar{1}7]$ direction and therefore at an angle of $11°30'$ with respect to the tetragonal c axis, and the total magnetic moment is about $3.8\mu_B$. The magnetic anisotropy energy (MAE) of CoO has been computed by Kanamori[34] who predicted that the magnetization is along [001] axis with a possible two degrees deviation. Nagamiya and Motizuki[35] modified his model and concluded that the magnetic axis might deviate as much as 10° from the c axis of the tetragonal structure.

Recent experimental x-ray absorption spectroscopy at the Co $L_{2,3}$ edges in CoO layers grown on different substrates shows substantial changes in its magnetic properties.[36] In particular, the experiment revealed that the magnitude and orientation of the magnetic moment depends on the strain on the CoO films induced by silver or MnO substrates. Layers of CoO grown on silver substrate show a slight contraction of the in-plane tetragonal lattice parameter which results in the total magnetic moment aligned in plane. On the contrary, MnO substrate expends the in-plane lattice parameter and as a consequence the magnetic moment rotates out of plane.

In the present study, we address the fundamental question regarding the effect of the substrate strain on magnetic properties of CoO. We first analyze the effect of strain on the MAE using a crystal-field theory (CFT) including the SOC to couple the strong orbital and spin moments. We then use *ab initio* approaches based on both the GGA and GGA+U methods to compute the magnetic properties and MAE. The latter method is used to handle the strongly correlated electronic structure of the CoO caused by the localized open d shell. We show in this study that the GGA+U method is able not only to reproduce the insulating AFM ground state of CoO but also the different orientations of the magnetic moment under effect of silver or MnO substrate strain whereas the GGA method is not. We found also that the results of the crystal-field analysis are in good agreement with the GGA +U results and experiment.

The paper is organized as follows, we first describe the CFT used to model the MAE of CoO under various substrate strains, then we discuss the results of the model. In the second part of the paper we introduce our GGA and GGA+U methods of calculation as implemented in the full-potential linear augmented plane-waves (FLAPW) FLEUR code[37] and show the band structure and magnetic properties of the AFM ground state of CoO. In the last section we compute and discuss the MAE results and compare them to our crystal-field results and other theoretical and experimental data.

II. CRYSTAL-FIELD APPROACH

In a partially filled atomic shell several electronic configurations (multiplets) are possible with different term energies due to Coulomb interaction. This Coulomb interaction is often expressed in terms of Slater integrals or equivalently Racah parameters. In a solid, the term F^0 is largely screened due to the polarization effect while higher-order terms are less screened.[38,39] This means that transition-metal ions in a solid still keep much of their atomic character. First, we consider a Co^{++} ion with d^7 in its ground state ^4F, which satisfies Hund's rules and corresponds to the highest total spin and highest orbital momentum. The first excited state is the ^4P term located at about 1.88 eV.[40] Hereafter we will consider only the ^4F terms relevant to our investigation concerning the magnetic anisotropy.

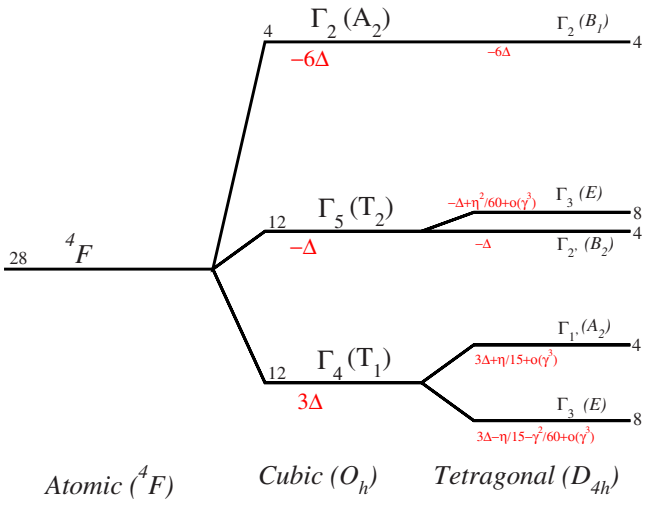

FIG. 2. (Color online) Decomposition of ^4F terms under cubic crystal field O_h (432), SOC, and tetragonal crystal field D_{4h} (422) into irreducible representations in Koster notation with the corresponding energy splittings.

In its paramagnetic state CoO assumes the NaCl structure so that Co^{++} form an fcc lattice surrounded by an octahedron formed by the nearest-neighbor oxygen atoms as shown in Fig. 1. Below the Néel temperature antiferromagnetic CoO is subjected to a small tetragonal distortion. This distortion becomes more important in the case of CoO films grown on silver or MnO substrates. In the case of MnO substrate the CoO shows an in-plane elongation of about 4%.[36] In addition to these elastic effects, the reported value of the orbital magnetic moment in a neutron-scattering experiment of $1\mu_B$ (Ref. 32) leads to a strong coupling between the spin and spatial degrees of freedom via the SOC. In the antiferromagnetic phase below its Néel temperature, the magnetic exchange coupling between the two sublattices of Co^{++} in CoO mediated by the superexchange can be described approximately by the Heisenberg model (in the limit of strong correlated electrons), where the exchange coupling depends inversely on U and is proportional to the square of the hopping integral (Anderson term).

A. Spin-independent Hamiltonian

In this part we neglect both the SOC and the exchange coupling. The free ion Co^{++} is perturbed by the cubic crystal fields. In the cubic symmetry the Hamiltonian is written as

$$H = V_0 + 11\sqrt{\pi}\Delta\left\{y_4^0(\hat{r}) + \sqrt{\frac{5}{14}}[y_4^4(\hat{r}) + y_4^{-4}(\hat{r})]\right\} + o(r^4), \tag{1}$$

where V_0 is the spherical part of the potential, Δ is a constant representing the cubic crystal field, and y_l^m are the spherical harmonics. The ^4F term splits into two orbital triplets Γ_4, Γ_5 and one orbital singlet Γ_2 (Throughout this paper we will use the irreducible representations $\Gamma_1 \cdots \Gamma_5$ of the cubic symmetry O_h in absence of spin-orbit coupling and $\Gamma_6 \cdots \Gamma_8$ where spin orbit is considered.) (Refs. 41 and 42) localized at 3Δ, $-\Delta$, and -6Δ, where $\Delta \approx -0.262$ eV.[43,44] To take the tetragonal distortion into account we can show that the deviation from the cubic crystal field ΔV can be written as

$$\Delta V(\vec{r}) = \eta\left[\frac{\delta a}{a_0} - \frac{\delta c}{a_0}\right] y_2^0(\hat{r}) + O\left(\frac{r^4}{a^5}\right) \approx \eta\gamma y_2^0(\hat{r}), \tag{2}$$

where

$$\gamma = \frac{\delta a}{a_0} - \frac{\delta c}{a_0}, \tag{3}$$

η is a constant representing the tetragonal crystal field, and a_0 is the lattice parameter for cubic (NaCl) structure, $\delta a = a - a_0$ and $\delta c = c - c_0$ (a and c being the lattice parameters of the tetragonal structure).

Kanamori[34] has estimated that η is about 0.124 eV and produced about 1% strain at low temperatures. Here, we estimated η from the reported experimental value of elastic stiffness constant C_{11} (Refs. 45–47) assuming that the change in the total energy is due to a uniaxial stress translated completely to a tetragonal variation in the potential and that the equilibrium volume corresponds to the experimental one. This leads to a value of η around 0.0235 eV per 0.6% of the variation in the volume. The sign of the tetragonal potential ΔV is determined by the sign of γ [see Eq. (3)].

In first order, under the tetragonal distortion, Fig. 2 shows that the orbital triplet Γ_4 splits into an orbital singlet $\Gamma_{1'}$ and an orbital doublet Γ_3. While the triplet Γ_5 splits into an orbital singlet $\Gamma_{2'}$ and an orbital doublet Γ_3 in second order. The highest singlet Γ_2 does not split. The lowest level is Γ_3 for $\gamma > 0$ and $\Gamma_{1'}$ for $\gamma < 0$. Using group theory and exact diagonalization we show that the wave function corresponding to the doublet $\Gamma_3(E)$ are of the form

$$\psi_E(\hat{r}) = \sqrt{\frac{5}{8}} y_3^{\pm 3}(\hat{r}) - \sqrt{\frac{3}{8}} y_3^{\mp 1}(\hat{r}) \tag{4}$$

while that of the singlet $\Gamma_{1'}(A_2)$ is of the form

$$\psi_{A_2}(\hat{r}) = y_3^0(\hat{r}). \tag{5}$$

At this stage we showed that due to compression along c axis ($c < a_0 < a \Leftrightarrow \gamma > 0$) the orbital moment is $\pm 1.5\mu_B$. However if $c > a_0 > a$ the orbital moment is zero. We will see in the next section that adding the SOC will mix these two states. We also notice also that in the case of CoO strained by silver substrate the GGA+U computed orbital moment is much smaller than that for the CoO strained by MnO substrate in agreement with our model and the experimental results.[36] It remains now to switch on the SOC and calculate the MAE of CoO subjected to a tetragonal distortion.

B. Spin-orbit coupling

In this section we investigate the effect of the SOC on magnetic properties of CoO. First the spin-orbit Hamiltonian in spherical symmetry is given by

$$H_{\mathrm{SOC}} = \lambda \vec{L} \cdot \vec{S}. \tag{6}$$

The reported experimental and calculated values[36,48] of the spin-orbit coupling strength λ range between -0.07 to

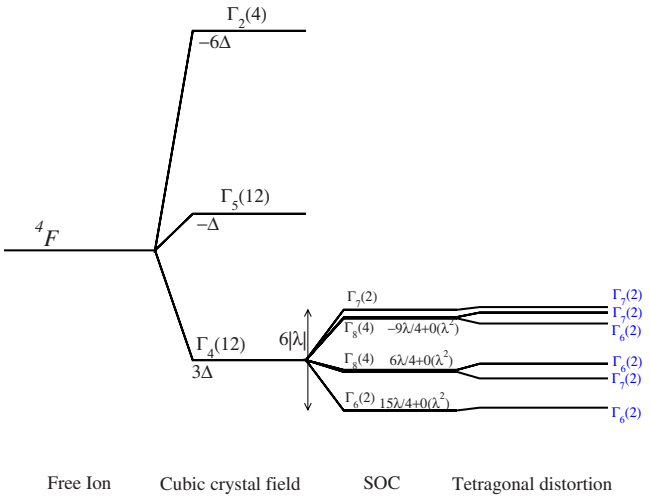

FIG. 3. (Color online) Decomposition of ^4F term under cubic crystal field O_h (432) and tetragonal crystal field D_{4h} (422) into irreducible representations in Koster notation (and Mulliken notation) with corresponding energy splittings.

−0.02 eV. The SOC strength (λ) is negative for more than half field d atomic shell (see Sec. III where our calculated value is found to be −0.07 eV). We will use group theory to discuss the two limits, i.e., $\eta \ll \lambda$ and $\lambda \ll \eta$ and diagonalize the Hamiltonian exactly for all cases.

In the case where $\eta \ll \lambda$, the spin function belongs to $D^{3/2}$ or to Γ_8 of the O_h group, so it is the tensor product of the irreducible representations (IRPs) Γ_4, Γ_5, and Γ_2 of the group O_h and Γ_8 is

$$\Gamma_4 \otimes \Gamma_8 = \Gamma_6 + \Gamma_7 + 2\Gamma_8,$$

$$\Gamma_5 \otimes \Gamma_8 = \Gamma_6 + \Gamma_7 + 2\Gamma_8,$$

$$\Gamma_2 \otimes \Gamma_8 = \Gamma_8,$$

where $\otimes$ is the tensor product. Hereafter, we limit the discussion to the lowest orbital triplet Γ_4. The IRP Γ_6 and Γ_7 are doubly degenerate, $\chi_{\Gamma_6(\Gamma_7)}(E)=2$ while Γ_8 is a quadruplet (see Fig. 3). If the SOC is treated in first-order perturbation instead, the orbital triplet will split into one singlet one doublet and one triplet.[49] The singlet Γ_6 is lowered in energy by $\frac{15}{4}|\lambda|$, the doublet Γ_8 is lowered by $\frac{6}{4}|\lambda|$, while the highest double Γ_8 and singlet Γ_7 are close in energy and pushed up by $\frac{9}{4}|\lambda|$. This splitting by the SOC leads to a width of the first peak in neutrons scattering on the order of $6|\lambda|$ in the paramagnetic phase where the deviation from the NaCl structure is supposed to be negligible. The tetragonal distortion splits further the quadruplet Γ_8 to two Kramer's doublets $\Gamma_6+\Gamma_7$. No further splitting will occur under any additional crystal *electric* field.

In the case where $|\lambda| \ll \eta$, the lowest level Γ_3 and $\Gamma_{1'}$ of Fig. 3 split into three Kramer's doublet Γ_6 and three Kramer's doublet Γ_7. Notice that because of the SOC the orbital moment is quenched by mixing the states y_3^m with $y_3^{m\pm1}$. Using group theory, crystal *electric* fields plus the SOC lead, at the end, to the splitting of the lowest cubic level Γ_4 to $3\Gamma_6$ and $3\Gamma_7$. After discussing the effect of crystal field and SOC effects on the ionic ground state ^4F we will discuss in the next section the effect the exchange coupling and will calculate the MAE below the Néel temperature.

C. Magnetic exchange and magnetic anisotropy energy

In Sec. II B, we restricted the spin as a vector along the z direction because the SOC was omitted in our calculation. Let us now include the SOC and assume that the direction of the magnetization is along a unit vector $\vec{u}$ described by two angles, an inclination angle ϑ and an azimuthal angle φ. The MAE is the difference between ground-state energies for two different orientations of the magnetization. We can show that the MAE is zero if we do not take in account the exchange splitting. In order to have magnetic anisotropy *we need in addition of the SOC the magnetic exchange coupling*.

Now we consider two Co^{++} ions interacting antiferromagnetically and subjected to the same crystal field. The magnetization for the first ion points along a $\vec{u}$ characterized by (ϑ, φ) and the second in $(\pi-\vartheta, \pi+\varphi)$. The two spin interact via a Heisenberg-type Hamiltonian

$$H_{exc} = J\vec{S}_{\vec{u}}^{(1)}\vec{S}_{-\vec{u}}^{(2)}, \tag{7}$$

where $J>0$ leading to an antiferromagnetic coupling between Co^{++} ions.

Figure 4(a) shows the variation in the MAE of CoO under strain along the c axis. We show that for $\gamma<0$ the easy axis

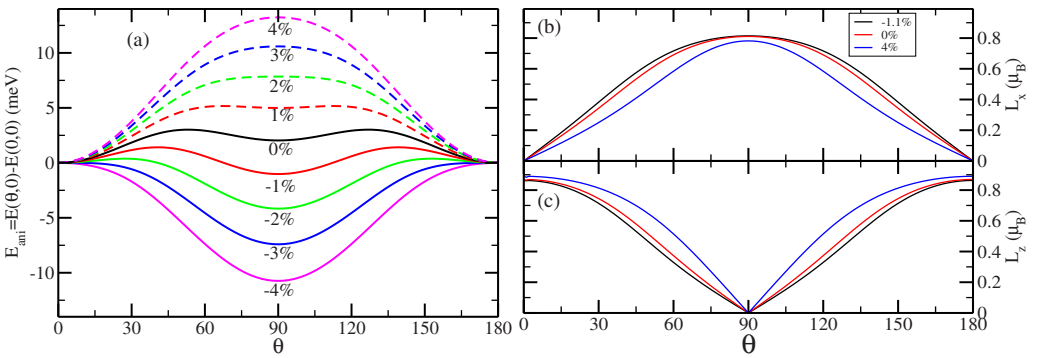

FIG. 4. (Color online) (a) Variation in the magnetic anisotropy energy, (b) the in-plane orbital moment, and (c) the out-of-plane orbital moment with ϑ taking $\varphi=0$ for different tetragonal distortions. The percentage corresponds to the values of γ [see Eq. (3)].

is out of plane ($\vartheta=0$). For a perfect cubic symmetry ($a=c$ or $\gamma=0$) the value of the MAE is found to be 2.03 meV when we take the values $\Delta=-0.25$ eV, $\lambda=-0.0225$ eV, and $\eta=0.0235$ eV. This value of MAE increases with increasing the γ ratio. The MAE reaches 13.2 meV for $\gamma=4\%$ which corresponds to the tetragonal structure of CoO grown on MnO substrate.[36] In case where $\gamma<0$, the easy axis rotates from out of plane to in plane ($\vartheta=\pi/2$). For $\gamma=-1.1\%$ (case of CoO grown on silver substrate) our calculated value is -1.8 meV.

The variation in the orbital moment is also presented in Figs. 4(b) and 4(c) which shows that out-of-plane orbital moment (L_z) vanishes for a zenith angle (ϑ) of $\pi/2$ and reaches its maximum for $\vartheta=0$ and π. The in-plane orbital moment (L_x) has a quadrature phase relationship to L_z and it reaches its maximum for $\vartheta=\pi/2$. The orbital moment $\vec{L}$ remains always in the plane xz and almost parallel to $\vec{S}$. The maximum value of the orbital moment depends on the value of the tetragonal distortion, and it is $0.86\mu_B$, $0.87\mu_B$, and $0.89\mu_B$ for CoO/Ag, CoO, and CoO/MnO systems, respectively. As discussed in the previous section, the presence of the SOC leads to a reduction in the orbital moments below $1\mu_B$. The value of the orbital moment increases only if the higher orbitals were taken into account. This will correspond to a situation where the tetragonal distortion η or the SOC strength λ is comparable to the cubic crystalline field Δ.

We showed in this section by using a simple model based on CFT that first the orbital moment for CoO cannot exceed $1.5\mu_B$ which is the maximum orbital moment of all splitted states of the triplet ground state Γ_4. Second, in the absence of the exchange magnetic coupling magnetocrystalline anisotropy will not occur. Finally, the presence of such coupling combined with the tetragonal distortion lead to the switching of the magnetization easy axis of CoO from out of plane to in plane depending on the ratio a/c.

The atomic approach used in this section is based on parameters such as Δ, η, and λ, and their values were extracted from experiment. In the next section, we will use the density-functional theory to describe the electronic structure of CoO, where the only parameter is the size of the Coulomb interaction among the Co $3d$ electrons.

III. *AB INITIO* CALCULATIONS

A. Method of calculation

In this part, we used the FLAPW method[50,51] as implemented in the code FLEUR,[37] within the GGA (Ref. 52) combined with the on-site Coulomb repulsion (GGA+U) to describe the strong electronic correlation of CoO,[15] where the double-counting term is taken to satisfy an *atomiclike* limit of the local-density approximation (LDA) total energy.[16] The calculation for GGA+U have been performed for different values of the parameters U while the parameter J is kept fixed to 0.92 eV.[10] The SOC is included in second variation manner, where one has first to determine the Kohn-Sham eigenvalues by diagonalizing the scalar relativistic Hamiltonian H_0 that includes only the Darwin and mass-velocity relativistic terms. The calculation is similar to our most recent calculation of Gd,[53] where the spin-orbit contribution

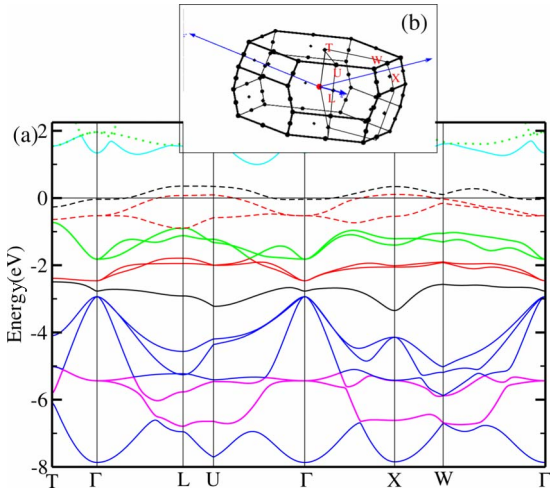

FIG. 5. (Color online) (a) Band structure of the rhombohedral structure of CoO AFM-II ($R\bar{3}m$) using GGA and (b) its rhombohedral Brillouin zone.

H_{SOC} to the Hamiltonian is computed along the quantization axis **u** defined by its polar angles ϑ and φ.

The values of SOC parameter are calculated self-consistently for both cobalt and oxygen. Its value for the cobalt d states is -0.07 eV. Although, the value of λ for the cobalt p orbitals is much bigger (-0.43 meV) it has a negligible contribution to the Hamiltonian because of the reduced spin and orbital moments associated to p states. Moreover, for the oxygen the value of λ is about -0.029 eV and it has as well a negligible contribution. The diagonalization of the full Hamiltonian produces the eigenvalues and the eigenvectors as a linear combination of the Bloch wave functions of H_0. The plane-wave cutoff for the basis functions $K_{max}=4.1$ a.u.$^{-1}$, the charge density and potential cutoff $G_{max}=12.30$ a.u.$^{-1}$, the muffin-tin radii R_{mt} is set to 2.23 a.u. for Co and 1.73 a.u. for oxygen. The wave functions as well as the charge density and the potential inside the muffin-tin spheres were expanded up to $l_{max}=8$. The convergence of the MAE is obtained using about 12500 **k** points in the full Brillouin zone (BZ) (see Fig. 9 for the convergence test).

The calculation were performed using the Bravais lattice vectors $(a,a/2,c/2)$, $(a/2,a,c/2)$, $(a/2,a/2,c)$, leading to a rhombohedral structure in case where $a=c$ and a triclinic in case of $c\neq a$. All calculations we done using the experimental lattice parameters[36] for bulk CoO, CoO/Ag, and CoO/MnO. In terms of these Bravais vectors, the cobalt atoms are at (0,0,0) and (1/2, 1/2, 1/2) and the oxygen atoms at (1/4, 1/4, 1/4) and $(-1/4, -1/4, -1/4)$.

B. Electronic structure

For a better understanding of the role of the electron-electron correlation on the electronic structure of the cobalt monoxide, we investigate the band structure in the rhombohedral (trigonal) unit cell (D_{3d}) of the AFM-II magnetic structure using GGA (Fig. 5) and GGA+U (Fig. 6). In the rhombohedral symmetry, as mentioned before, the d orbitals split into two doublet e_g and e_g' and a singlet a_g (e_g' and a_g correspond to the cubic splitting t_{2g}).

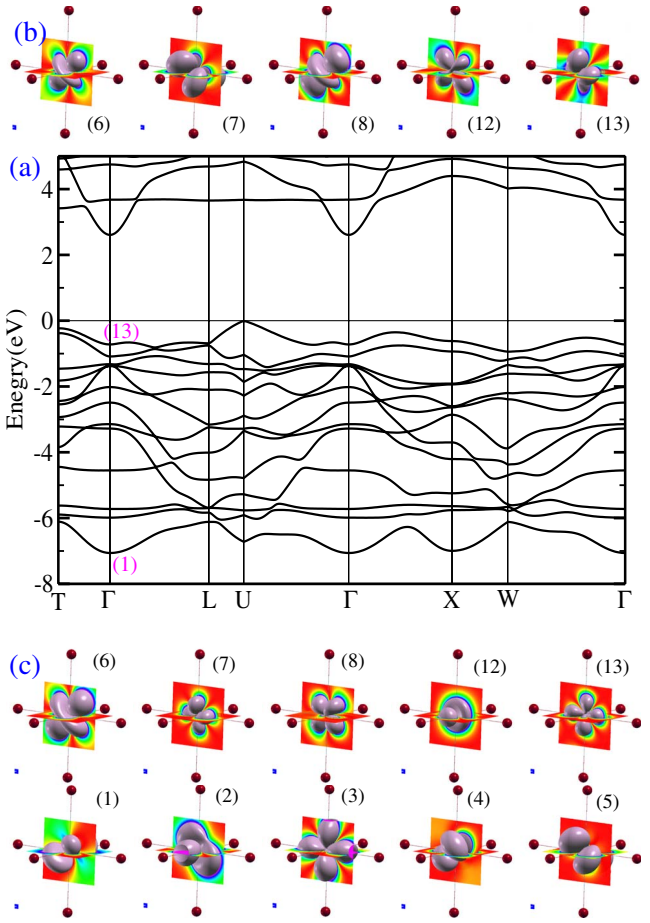

FIG. 6. (Color online) (a) Band structure of the rhombohedral structure of CoO AFM-II ($R\bar{3}m$) using GGA+U (U=6.2), (b) Co minority electron density, and (c) Co majority electron density at Γ point for different bands.

In Fig. 5, we show the band structure obtained using the GGA. It shows that CoO is metallic where the Fermi level lies in the middle of the cubic orbital $t_{2g}(e_g'+a_g)$ which is partially occupied. The O $2p$ orbitals, presented in blue lines (bands between −8 and −3 eV), are the lowest bands with a bandwidth of 5 eV, they are coupled to the e_g orbitals of Co d (magenta) at about −6 eV. The spin-up singlet a_g (black solid line) and the doublet e_g' at about −2 eV (red solid line) spread over an energy window of 1.5 eV width. They lie at about −3 eV below the Fermi level (E_F). The remaining of majority e_g just above −2 eV (green lines) lies above the $t_{2g}=e_g'+a_g$ by about 0.7 eV (at the Γ point) and with a bandwidth of ≈1 eV. For the minority-spin singlet a_g near 0 eV (black dashed line) and the doublet e_g' (red dashed line) just below a_g cross the Fermi level and have a bandwidth of 1.3 eV. The spin-down doublet e_g (cyan dashed line) just below a_g lies at 1.9 eV above E_F and it is narrower than its spin-up counter partly by about 0.4 eV. The exchange splitting is about 2.0 eV. All the Co d manifold (e_g', e_g, and a_g) have an average bandwidth of 1.2 eV. When the on-site Coulomb repulsion U is included, it leads a huge change in the electronic structure, not only by pushing the bands up and down in energy depending on their occupations, but also by changing the symmetry of each band. In Fig. 6(a), we show the band structure

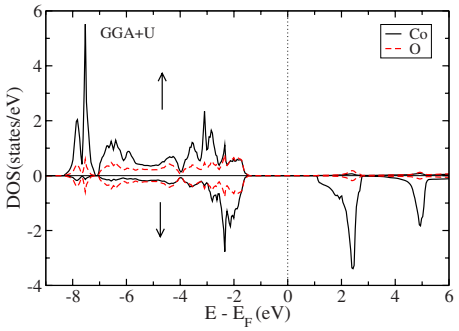

FIG. 7. (Color online) Density of states of CoO in the AFM-II phase calculated using GGA+U, U=6.2 eV.

obtained within the GGA+U with U=6.2 and J=0.92 eV and the associated orbitals at the gamma point, Figs. 6(b) and 6(c) (the spin-dependent atomic-orbital contributions for each energy level at the Γ point calculated for both GGA and GGA+U are given in the supplementary information (see Ref. 63). It is known that the presence of the on-site Coulomb energy leads to a further reduction in the system [see Eq. 16 of Ref. 15]. The lowest band is mainly a hybridization between the O $2p$ orbitals and d_{xz} and d_{yz} (35%). The second and the third lowest band located at −5 to −6 eV are mainly (72%) the localized doublet (e_g) of Co. The singlet and the doublet are spread over an energy range of ≈2 eV (fourth to eighth bands). The O $2p$ orbitals are now located at 1.5 eV below the Fermi level (ninth to 11th bands). The U reduces the hybridization between the O p and Co d orbitals. The lowest-unoccupied band is the s orbital of the Co atoms which lies at about 2.5 eV above E_F. The singlet a_g, now a linear combination of d_{xz} and d_{yz}, is situated at 3 eV. The doublet e_g is now between 4.6 and 5 eV above the E_F.

As the band structure shows, even if the geometrical structure of the antiferromagnetic-type-II CoO is a D_{3d}, the presence of a strong U splits the $3d$ manifold into five singlets (no double degeneracy). The tetragonal distortion in the CoO will further accentuate such a lift of degeneracy.

Figure 7 shows the density of state of the distorted structure of the cobalt monoxide with c/a ratio of 0.988 (hereafter referred as bulk CoO) calculated using the GGA+U. It shows the same structure details as discussed in the rhombohedral case.

The band gap depends strongly on the value of U, passing from zero in the GGA calculation to about 3 eV for U =7 eV. The Coulomb repulsion leads to an indirect band-gap insulator. The indirect gap, between the top of the valence band at the high symmetry U point and the bottom of the conduction band at the Γ point, is about 2.44 eV for U =6.2 eV. The direct band gap corresponding to the optical gap (in absence of excitonic effects) is larger by about 0.6 eV and occurs at both U and Γ high symmetry points.

The calculated value of the magnetic moment depends slightly on the value of U used, it ranges between 2.70μ_B and 2.74μ_B for realistic values of U between 6.2 and 8.3 eV. These values are in agreement with other reported calculations but are far from the measured values. The discrepancy between theory and experimental is due to the unquenched orbital moment which contributes to the total magnetic mo-

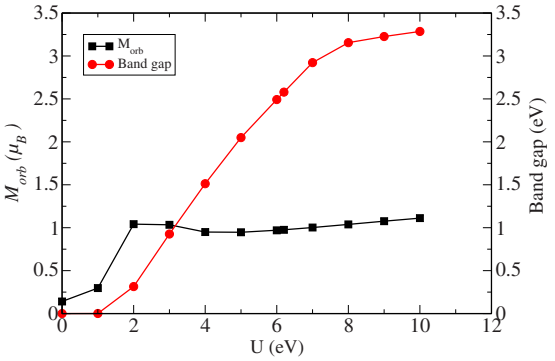

FIG. 8. (Color online) Variation in the orbital magnetic moment and the band gap as a function of the Hubbard parameter U using GGA+U+SOC.

ment by as much as $1\mu_B$ as suggested by Svane *et al.*[6] and Anisimov *et al.*[10] The presence of the orbital moment is due to the SOC believed to be small in early transition metals. The SOC combined with a strong correlations leads to an orbital magnetic moment of about $1.0\mu_B$ for $U=6.2$ eV (see Fig. 8) compared to only $0.17\mu_B$ obtained using the GGA approach. This value is in good agreement with the measured experimental value.[33] Table I shows our calculations compared to various theories[6,9,22,54,55] and experiments.[23,25,54,56–58]

In Fig. 9, the orbital moment as well as the band gap are plotted versus the strength of the on-site Coulomb interaction. The band gap increases continuously with increasing U and levels off for $U=8$ eV while the orbital moment is quenched for small value of U and increases to reach a value $1\mu_B$ for U equals to about 2 eV and shows a saturation for all higher values of U up to 10 eV.

C. Magnetocrystalline anisotropy of CoO under substrate strain

A great deal of theoretical work has been devoted to the calculation of the MAE, either using the total-energy (TE) approach or the force theorem (FT) (Refs. 59 and 60) approach. The MAE can be calculated as a difference in the total energy for out-of-plane and in-plane magnetizations. The order of magnetocrystalline anisotropy requires a high sampling in the BZ and an accurate band-structure calculation.

Figure 9 shows the convergence of MAE versus the number of k points in the BZ. It can be seen that one needs more than 12 000 k points in the first BZ to converge the MAE versus k-point sampling. Using a classical dipolar interaction, the shape anisotropy contribution was found to be negligible and independent of the method used in calculating the electronic structure. Indeed we have found it to be 0.5 μeV in the GGA and 1 μeV in the GGA+U. These results are in agreement with other dipolar calculation.[61]

We have calculated the MAE both within the GGA and GGA+U. Figure 10 shows our calculation for bulk CoO versus the inclination angle θ and for different azimuthal angle

TABLE I. Calculated spin m_s, orbital m_l, and total m_T magnetic moments (in μ_B) and energy band gap (E_g) of CoO bulk, CoO/Ag(001), and CoO/MnO(001) within the GGA and the GGA+U. The SOC is included in both methods. The results are compared to other calculations and experiments.

Material	Method	m_s	m_l	m_T	E_g (eV)
Bulk	GGA	2.45	0.17	2.62	0.0
	GGA+(U=6.2 eV)	2.70	1.0	3.7	2.44
CoO/Ag	GGA	2.45	0.16	2.61	0.0
	GGA+(U=6 eV)	2.68	0.45	3.13	2.44
CoO/MnO	GGA	2.40	0.17	2.60	0.0
	GGA+(U=7.1 eV)	2.70	0.83	3.53	2.44
Bulk	Other calc. LSDA	2.37[a] 2.3[b] 2.41[c], 2.33[d]	0.31[a] 2.12[d]	2.72[a] 4.53[d]	0[d]
Bulk	Other calc. LDA+U	2.74[b] 2.53[d]	1.19[d]; 1.05[e]	3.72[d], 3.75[e]	2.45[b], 2.81[d]
Bulk	Expt.		1[e,f]	3.35[g], 3.80[e,f], 3.98[h]	2.6[h], 2.4[i]
CoO/Ag	Expt.[j]	2.14	1.00	3.14	
CoO/MnO	Expt.[j]	2.46	1.36	3.82	

[a]Reference 9 (spin-polarized LDA with SOC).
[b]Reference 22 (LDA+U with U=5 eV).
[c]Reference 55 (spin-polarized LDA with orbital polarization).
[d]Reference 6 (SIC to the LDA).
[e]Reference 54 (LDA+U with U=8 eV).
[f]Reference 25.
[g]Reference 57.
[h]Reference 58.
[i]Reference 23.
[j]Reference 56.
[k]Reference 36.

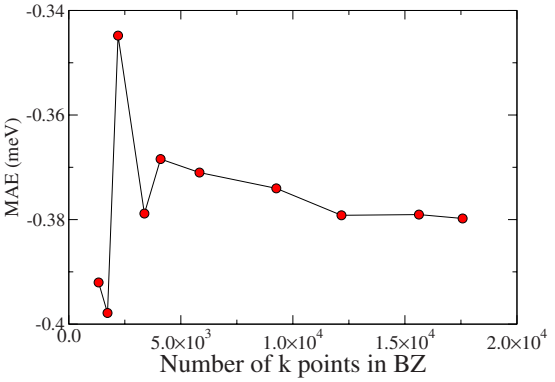

FIG. 9. (Color online) Convergence of the MAE as a function of the number of **k** points in the BZ calculated within the GGA.

φ both within the GGA (left panel) and GGA+U (right panel). The GGA leads to a magnetization, the inclination angle θ of 66° and the azimuth angle φ of 45° and the hard axis along the c direction, with a MAE of 0.6 meV in disagreement with experiment, whereas in GGA+U the easy plane is out of plane with a MAE of 2.2 meV. The GGA+U calculations are performed using U equal to 6.2 eV in order to reproduce the experimental band gap. The GGA+U value agrees with that calculated by Haverkort.[62] However the experimental easy axis is $[\bar{1}\bar{1}7]$ and makes therefore an angle of about 11°30′ with the z axis[25] in slight disagreement with our calculation. Such an easy axis is inconsistent with the uniaxial tetragonal symmetry and a multispin-axis magnetic structure was suggested to explain this result. The multispin-axis magnetic structure is consistent with the tetragonal lattice distortion.[25] An easy cone is also possible if the energy of thermal fluctuations is greater than the azimuthal angle φ dependence of the MAE.

CoO under substrate strain

In this section we study the magnetic properties and MAE of CoO/Ag(001) and CoO/MnO(001) systems and we grouped the results, respectively, in Tables I and II. The lattice constant of bulk Ag(4.09 Å) is smaller than that of the bulk CoO(4.26 Å) and the MnO(4.444 Å) is larger than the one of the CoO. We therefore expect that the in-plane lattice parameter of CoO on silver to be compressed and that of CoO on MnO to be expended. These strain effects have been recently observed by Csiszar *et al.*[36] who found using x-ray diffraction that the CoO on silver is slightly compressed in plane ($a_{\parallel}$=4.235 Å, $a_{\perp}$=4.285 Å) and from reflection high-energy electron diffraction that CoO sandwiched by MnO is about 4% expanded in plane ($a_{\parallel}$=4.424 Å). Our objective is therefore to study the effect of the strain on the magnetic properties and magnetic anisotropy of CoO by means of both GGA and GGA+U and including in both calculation the SOC. Our results will be compared to the experimental results of Csiszar *et al.*[36]

TABLE II. Calculated magnetic anisotropy energy in millielectron volt for CoO bulk, CoO/Ag(001), and CoO/MnO(001) using the force theorem within GGA, GGA+U, and CFT. The results are compared to other calculations and experiment (Refs. 36 and 62).

Method	CoO/Ag (U=6 eV)	CoO (U=6.2 eV)	CoO/MnO (U=7.1 eV)
GGA	0.3	−0.4	4.8
GGA+U	−2.2	2.5	9.3
CFT	−1.1	2.9	13.0
Other calculations	−1.6[a]	2.3[b]	4.8[a]

[a]Reference 36.
[b]Reference 62.

In case of CoO/Ag(001), where the ratio c/a is slightly larger than one [$\gamma<0$ Eq. (3)], we used both the GGA and GGA+U, with an on-site Hubbard parameter U=6 eV. From the TE calculations using the GGA approach, we find that the easy axis is perpendicular to the growth plane (z axis) and the hard axis is in plane. The calculated spin magnetic moment is 2.45μ_B and an orbital magnetic moment of 0.16μ_B. The value of the total magnetic moment is smaller than that obtained by Csiszar *et al.*[36] The MAE is 0.27 meV in the self-consistent total-energy calculations, which is smaller and with opposite sign to that obtained by Csiszar *et al.*[36] (−1.6 meV). Including the on-site Coulomb repulsion [with U=6 eV this value gives the same experimental energy band gap of about 2.4 eV for CoO (Ref. 56)] the spin magnetic moment is increased to 2.68μ_B as well as the orbital magnetic moment (0.45μ_B) leading to a total magnetic

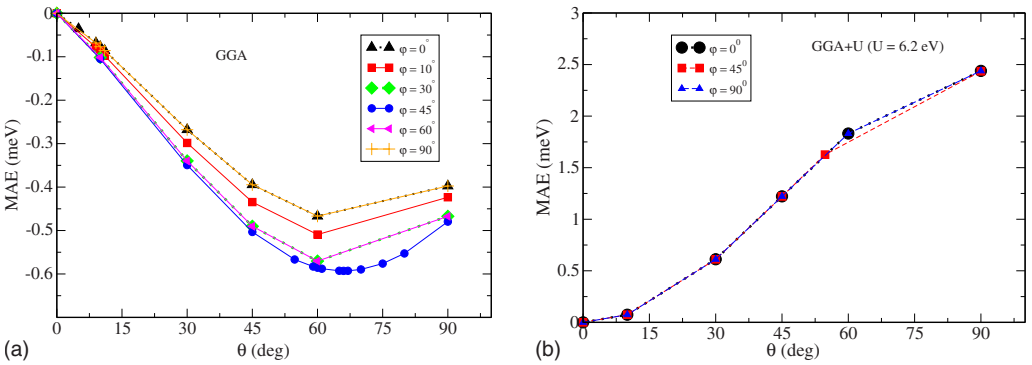

FIG. 10. (Color online) Calculated MAE as a function of the inclination angle (ϑ) for various azimuthal angles (φ). The left panel represents the GGA calculation where the easy axis is almost in plane (the azimuthal angle φ=45 and the inclination angle ϑ=66. On the contrary, for the GGA+U calculation the easy axis is out of plane in better agreement with experiment.

moment of $3.13\mu_B$. This value is in good agreement with the value obtained by Csiszar *et al.*[36] ($3.14\mu_B$). From both calculations, FT and TE, we showed that the easy axis is in plane and that the hard axis is out of plane. The MAE calculated using the FT approach is on the order of −2.49 and −2.40 meV using the TE (MAE=$E_{(x,y)}-E_z$). These values agree with value of −1.6 meV obtained by Csiszar *et al.*[36] and with the value of −1.1 meV obtained by the CFT model exposed in Sec. II (see Table II).

A quantitative comparison of the CFT and the GGA+U method in order to understand why both methods provide similar results is a challenging task and is beyond the scope of this paper. In the CFT we considered just a single ion isolated and a pure ^4F state, which is too simplified. On the other hand the *ab initio* wave function is complicated and only the charge density is meaningful and can be related to the many-body problem. However, at the qualitative level, the agreement of the crystal-field approach and the GGA+U is due to the fact that the GGA+U localizes the d electron much more than the GGA, leading to an enhanced atomic character of the d orbitals.

In the case of CoO/MnO(001) the c/a is less than 1 [$\gamma > 0$ Eq. (3)] and we use the value of Hubbard parameter, U=7.1 eV (this value reproduces the experimental energy gap[56] of CoO). We obtained the same values of the spin magnetic moments, $2.40\mu_B$ in the GGA and $2.70\mu_B$ in the GGA+U, as the ones obtained in the CoO/Ag(001). When including the SOC, the values of spin magnetic moment remain almost unchanged and the orbital magnetic moment is about $0.2\mu_B$ for GGA and a $0.83\mu_B$ for GGA+U. The values of the M_{orb} are smaller compared to those obtained by Csiszar *et al.*[36] In both methods we obtained the easy axis out of plane (c axis) and the hard axis in plane with a MAE of about 4.8 meV using the GGA and 9.3 meV using the GGA+U. These results are in good agreement with the values deduced from experiment by Csiszar *et al.*[36]

IV. CONCLUSION

In conclusion, we showed that a good description of the electronic structure and magnetic properties of CoO under strain requires the inclusion of the electron-electron correlations that are partially missed in LSDA or GGA. Such electronic correlations introduced by the on-site Coulomb repulsion (Hubbard parameter U) within the GGA+U method lead to a better description of the electronic structure of CoO. The GGA+U reproduced not only the band gap, the spin and orbital moments, but also the magnetic anisotropy energy and hence the orientation of the magnetic moment of CoO under strain caused by silver or MnO substrates. In fact, we have shown that the magnetization axis switches from out of plane to in plane due to strain on the in-plane lattice parameter of CoO induced, respectively, by silver or by MnO substrates, in good agreement with experiment. These results are also in good agreement with our crystal-field analysis. The latter analysis helped showing how the cubic e_g and t_{2g} orbitals split under tetragonal or rhombohedral symmetries caused by substrate strain and their effect on the magnetic anisotropy energy.

ACKNOWLEDGMENTS

We would like to acknowledge support from ANR PNANO Grant No. ANR-06-NANO-053 and the MESRS of Algeria for financial support. This work was performed using HPC resources from GENSI-CINES Grant gem1100.

[1] J. H. de Boer and E. J. W. Verwey, Proc. Phys. Soc. **49**, 59 (1937).
[2] N. F. Mott and R. Peierls, Proc. Phys. Soc. **49**, 72 (1937).
[3] N. F. Mott, *Metal-Insulator Transitions* (Taylor & Francis, London, 1974).
[4] O. K. Andersen, H. L. Skriver, H. Nohl, and B. Johansson, Pure Appl. Chem. **52**, 93 (1980); K. Terakura, A. R. Williams, T. Oguchi, and J. Kübler, Phys. Rev. Lett. **52**, 1830 (1984); K. Terakura, T. Oguchi, A. R. Williams, and J. Kübler, Phys. Rev. B **30**, 4734 (1984).
[5] J. P. Perdew, J. A. Chevary, S. H. Vosko, K. A. Jackson, M. R. Pederson, D. J. Singh, and C. Fiolhais, Phys. Rev. B **46**, 6671 (1992).
[6] A. Svane and O. Gunnarsson, Phys. Rev. Lett. **65**, 1148 (1990).
[7] Z. Szotek, W. M. Temmerman, and H. Winter, Phys. Rev. B **47**, 4029 (1993).
[8] M. Arai and T. Fujiwara, Phys. Rev. B **51**, 1477 (1995).
[9] M. R. Norman, Phys. Rev. B **40**, 10632 (1989).
[10] V. I. Anisimov, J. Zaanen, and O. K. Andersen, Phys. Rev. B **44**, 943 (1991); V. I. Anisimov, M. A. Korotin, J. Zaanen, and O. K. Andersen, Phys. Rev. Lett. **68**, 345 (1992); V. I. Anisimov, I. V. Solovyev, M. A. Korotin, M. T. Czyzyk, and G. A. Sawatzky, Phys. Rev. B **48**, 16929 (1993).
[11] V. I. Anisimov and O. Gunnarsson, Phys. Rev. B **43**, 7570 (1991).
[12] V. I. Anisimov, P. Kuiper, and J. Nordgren, Phys. Rev. B **50**, 8257 (1994).
[13] W. E. Pickett, S. C. Erwin, and E. C. Ethridge, Phys. Rev. B **58**, 1201 (1998).
[14] S. L. Dudarev, A. I. Liechtenstein, M. R. Castell, G. A. D. Briggs, and A. P. Sutton, Phys. Rev. B **56**, 4900 (1997).
[15] A. B. Shick, A. I. Liechtenstein, and W. E. Pickett, Phys. Rev. B **60**, 10763 (1999).
[16] I. V. Solovyev, P. H. Dederichs, and V. I. Anisimov, Phys. Rev. B **50**, 16861 (1994).
[17] A. I. Liechtenstein, V. I. Anisimov, and J. Zaanen, Phys. Rev. B **52**, R5467 (1995).
[18] O. Bengone, M. Alouani, P. Blöchl, and J. Hugel, Phys. Rev. B **62**, 16392 (2000).
[19] E. Engel and S. H. Vosko, Phys. Rev. B **47**, 13164 (1993).
[20] P. Dufek, P. Blaha, and K. H. Schwarz, Phys. Rev. B **50**, 7279 (1994).
[21] Pan Wei and Z. Q. Qi, Phys. Rev. B **49**, 10864 (1994).
[22] W. Zhang, K. Koepernik, M. Richter, and H. Eschrig, Phys. Rev. B **79**, 155123 (2009).
[23] W. Jauch, M. Reehuis, H. J. Bleif, F. Kubanek, and P. Pattison,

Phys. Rev. B **64**, 052102 (2001).
[24] M. D. Rechtin and B. L. Averbach, Phys. Rev. Lett. **26**, 1483 (1971).
[25] W. L. Roth, Phys. Rev. **110**, 1333 (1958).
[26] S. Saito, K. Nakahigashi, and Y. Shimomura, J. Phys. Soc. Jpn. **21**, 850 (1966).
[27] W. Jauch and M. Reehuis, Phys. Rev. B **65**, 125111 (2002).
[28] E. Uchida, N. Fukuoka, H. Kondoh, T. Takeda, Y. Nakazumi, and T. Nagamiya, J. Phys. Soc. Jpn. **19**, 2088 (1964).
[29] W. Neubeck, C. Vettier, F. de Bergevin, F. Yakhou, D. Mannix, L. Ranno, and T. Chatterji, J. Phys. Chem. Solids **62**, 2173 (2001).
[30] G. Ghiringhelli, L. H. Tjeng, A. Tanaka, O. Tjernberg, T. Mizokawa, J. L. de Boer, and N. B. Brookes, Phys. Rev. B **66**, 075101 (2002).
[31] C. Henry La Blanchetais, J. Phys. Radium **12**, 765 (1951).
[32] C. G. Shull, W. A. Strauser, and E. O. Wollan, Phys. Rev. **83**, 333 (1951).
[33] T. Jo and T. Shishidou, J. Phys. Soc. Jpn. **67**, 2505 (1998).
[34] J. Kanamori, Prog. Theor. Phys. **17**, 177 (1957); **17**, 197 (1957).
[35] T. Nagamiya and K. Motizuki, Rev. Mod. Phys. **30**, 89 (1958).
[36] S. I. Csiszar, M. W. Haverkort, Z. Hu, A. Tanaka, H. H. Hsieh, H. J. Lin, C. T. Chen, T. Hibma, and L. H. Tjeng, Phys. Rev. Lett. **95**, 187205 (2005).
[37] http://www.flapw.de/pm/index.php; see also S. Bluegel and G. Bihlmayer, in *Computational Nanoscience: Do it Yourself!*, edited by J. Grotendorst, S. Bluegel, and D. Marx (John von Neumann Institute for Computing, Juelich, 2006), Vol. 31, p. 85.
[38] J. Zaanen and G. A. Sawatzky, J. Solid State Chem. **88**, 8 (1990).
[39] D. van der Marel and G. A. Sawatzky, Phys. Rev. B **37**, 10674 (1988).
[40] O. Ney, M. Trzecieki, and W. Hübner, J. Phys.: Condens. Matter **17**, 7489 (2005).
[41] G. F. Koster, J. O. Dimmock, R. G. Wheeler, and H. Statz, *Properties of the Thirty-two Point Groups* (MIT Press, Cambridge, Massachusetts, 1963).
[42] M. S. Dresselhaus, G. Dresselhaus, and A. Jorio, *Group Theory: Application to the Physics of Condensed Matter* (Springer-Verlag, Berlin, 2008).
[43] W. Low, Phys. Rev. **109**, 256 (1958).
[44] M. R. Daniel and A. P. Cracknell, Phys. Rev. **177**, 932 (1969).
[45] C. Massobrio and M. Meyer, J. Phys.: Condens. Matter **3**, 279 (1991), and references therein.
[46] F. Tran, P. Blaha, K. Schwarz, and P. Novak, Phys. Rev. B **74**, 155108 (2006).
[47] Q. Guo, H.-K. Mao, J. Hu, J. Shu, and R. J. Hemley, J. Phys.: Condens. Matter **14**, 11369 (2002).
[48] R. Schlapp and W. C. Penney, Phys. Rev. **42**, 666 (1932).
[49] R. Newman and R. M. Chrenko, Phys. Rev. **115**, 1147 (1959).
[50] M. Weinert, E. Wimmer, and A. J. Freeman, Phys. Rev. B **26**, 4571 (1982).
[51] E. Wimmer, H. Krakauer, M. Weinert, and A. J. Freeman, Phys. Rev. B **24**, 864 (1981).
[52] J. P. Perdew, K. Burke, and M. Ernzerhof, Phys. Rev. Lett. **77**, 3865 (1996).
[53] S. Abdelouahed, N. Baadji, and M. Alouani, Phys. Rev. B **75**, 094428 (2007).
[54] I. V. Solovyev, A. I. Liechtenstein, and K. Terakura, Phys. Rev. Lett. **80**, 5758 (1998).
[55] M. R. Norman, Phys. Rev. Lett. **64**, 1162 (1990); **64**, 2466 (1990).
[56] R. J. Powell and W. E. Spicer, Phys. Rev. B **2**, 2182 (1970).
[57] D. Herrmann-Ronzaud, P. Burlet, and J. Rossat-Mignod, J. Phys. C **11**, 2123 (1978).
[58] D. C. Khan and R. A. Erickson, Phys. Rev. B **1**, 2243 (1970).
[59] A. R. Mackintosh and O. K. Andersen, in *Electrons at the Fermi Surface*, edited by M. Springford (Cambridge University Press, Cambridge, England, 1980).
[60] M. Weinert, R. E. Watson, and J. W. Davenport, Phys. Rev. B **32**, 2115 (1985).
[61] M. Finazzi and S. Altieri, Phys. Rev. B **68**, 054420 (2003).
[62] M. W. Haverkort, Ph.D. thesis, der Mathematisch-Naturwissenschaftlichen Fakultät der Universität zu Köln, 2005.
[63] See supplementary material at http://link.aps.org/supplemental/10.1103/PhysRevB.81.184432 for the orbital character of the energy bands at the Γ point.